Asian Journal of Pharmaceutical Sciences 19 (2024) 100904

Available online at www.sciencedirect.com

ScienceDirect

journal homepage: www.elsevier.com/locate/AJPS

Research Article

Functionalized lipid nanoparticles modulate the blood-brain barrier and eliminate α-synuclein to repair dopamine neurons

Xiaomei Wu[a], *Renxiang Yuan*[b], *Yichong Xu*[b], *Kai Wang*[b], *Hong Yuan*[b,c], *Tingting Meng*[b,c], *Fuqiang Hu*[b,c,*]

[a] *Department of Pharmacy, Ruijin Hospital, School of Medicine, Shanghai Jiaotong University, Shanghai 200000, China*
[b] *College of Pharmaceutical Science, Zhejiang University, Hangzhou 310058, China*
[c] *Jinhua Institute of Zhejiang University, Jinhua 321299, China*

ARTICLE INFO

Article history:
Received 9 August 2023
Revised 16 January 2024
Accepted 17 February 2024
Available online 12 March 2024

Keywords:
Blood-brain barrier
Lipid nanoparticles
Brain delivery facilitation
α-Synuclein
Parkinson's disease

ABSTRACT

The challenge in the clinical treatment of Parkinson's disease lies in the lack of disease-modifying therapies that can halt or slow down the progression. Peptide drugs, such as exenatide (Exe), with potential disease-modifying efficacy, have difficulty in crossing the blood-brain barrier (BBB) due to their large molecular weight. Herein, we fabricate multi-functionalized lipid nanoparticles (LNP) Lpc-BoSA/CSO with BBB targeting, permeability-increasing and responsive release functions. Borneol is chemically bonded with stearic acid and, as one of the components of Lpc-BoSA/CSO, is used to increase BBB permeability. Immunofluorescence results of brain tissue of 15-month-old C57BL/6 mice show that Lpc-BoSA/CSO disperses across the BBB into brain parenchyma, and the amount is 4.21 times greater than that of conventional LNP. Motor symptoms of mice in Lpc-BoSA/CSO-Exe group are significantly improved, and the content of dopamine is 1.85 times (substantia nigra compacta) and 1.49 times (striatum) that of PD mice. α-Synuclein expression and Lewy bodies deposition are reduced to 51.85% and 44.72% of PD mice, respectively. Immunohistochemical mechanism studies show AKT expression in Lpc-BoSA/CSO-Exe is 4.23 times that of PD mice and GSK-3β expression is reduced to 18.41%. Lpc-BoSA/CSO-Exe could reduce the production of α-synuclein and Lewy bodies through AKT/GSK-3β pathway, and effectively prevent the progressive deterioration of Parkinson's disease. In summary, Lpc-BoSA/CSO-Exe increases the entry of exenatide into brain and promotes its clinical application for Parkinson's disease therapy.

* Corresponding author.
E-mail address: hufq@zju.edu.cn (F. Hu).
Peer review under responsibility of Shenyang Pharmaceutical University.

https://doi.org/10.1016/j.ajps.2024.100904

1. Introduction

Parkinson's disease (PD) is the second leading neurodegenerative disorder in the world. The clinical first-line medication is dopamine replacement therapy, which is a symptomatic treatment. Up to now, no therapy can slow down or arrest the progressive deterioration of PD. But, informed by new insights into mechanisms of neuronal death, several promising strategies are being tested for disease-modifying potential [1,2]. Exenatide (Exe) is a licensed drug for the treatment of type 2 diabetes mellitus. It is a glucagon-like peptide 1 (GLP-1) receptor agonist. Accumulating evidence implicates that Exe has neuroprotective and regenerative effects on PD [3–6]. The clinical trial of Exe in the treatment of PD has achieved Phase III (NCT04232969). However, the existence of the blood-brain barrier (BBB) makes it difficult for therapeutics, especially macromolecular drugs, to enter the brain, which is why brain diseases are difficult to treat.

BBB refers to a "barrier" between blood vessels and brain parenchyma that selectively prevents exogenous substances from entering the brain. In contrast to the relatively permeable systemic capillaries, brain capillaries tend to have a low rate of transcytosis, only allowing lipophilic drugs with a molecular weight of less than 500 Da to enter across [7,8]. The reason why it is difficult for exogenous substances to enter the brain is the tight junctions (TJs) between brain endothelial cells. TJs include claudins, occludins, and zonula occludens, etc., among which claudin-5 is crucial for forming a paracellular barrier and its disruption increases BBB permeability [9]. Exe is a polypeptide consisting of 39 amino acids with a molecular weight of 4186.6 Da, and apparently, it cannot enter the brain parenchyma easily.

In recent years, techniques and methods for opening the BBB to promote efficient drug entry into the brain have emerged increasingly, which include focused ultrasound, osmotic pressure disruption, photodynamic therapy, hyperosmolar mannitol, lexiscan, bradykinin and its analogues, etc. [10–16]. However, some molecules can induce inflammatory and innate immune responses while opening BBB [17,18]. For example, intracarotid artery hyperosmotic mannitol (ICAHM) infusions are viewed as a simple drug delivery mechanism. While BBB disruption by ICAHM generates a transient sterile neuroinflammatory response marked by increased production of cytokines, chemokines, and trophic factors leading to activation of astrocytes, microglia, and macrophages [19]. Borneol can improve BBB permeability, and its effect is rapid, reversible, and harmless [20–25]. Due to the first-pass effect, the dosage of borneol is very high, from 15 mg/kg to 1 g/kg [26]. To reduce the dosage of borneol, we chemically linked borneol onto lipid nanoparticles (LNP) to increase BBB permeability with low dosage.

PD is a neurodegenerative disease closely related to age. One of the required neuropathology of PD is the abnormal deposition of α-synuclein in neuron cytoplasm, which first polymerizes into oligomers and eventually into Lewy bodies [27–29]. We used the MPTP (1-methyl-4-phenyl-1,2,3,6-tetrahydropyridine hydrochloride) model of 15-month-old male C57BL/6 mice, whose microenvironment in the brain is more similar to that of PD patients, to recapitulate neuropathology of PD accurately. Glycogen synthase kinase 3 beta (GSK-3β) is involved in modulating autophagy, and dysregulated GSK-3β activity is implicated in PD pathogenesis and promotion of Lewy body formation [30]. Studies have shown that inhibition of GSK-3β could prevent the expression and aggregation of α-synuclein, thus reducing the formation of Lewy body. GLP-1 receptor stimulation has been shown to activate AKT (Protein Kinase B) and AKT activation inactivates GSK-3β [31–34].

In recent years, more and more research has been done on drug delivery systems for the treatment of brain diseases, such as ionizable drug delivery systems for gene therapy and nucleic acid delivery systems [35,36]. With high biocompatibility, biodegradability and lipid composition features that promote transport across biological membranes, LNP are ideal nanocarriers for brain delivery. Major facilitator superfamily domain-containing protein 2 (Mfsd2a) is specifically expressed in the endothelium of BBB and lysophosphatidylcholine (Lpc) is the specific substrate of Mfsd2a [37–39]. Lpc, as one component of LNP, could target the brain well. In addition, chitosan (CSO) exerts a proton sponge effect in the microenvironment of PD lesions [40,41], which enables Exe to be released accurately at the lesion site.

In summary, lacking effective disease-modifying drugs and BBB preventing macromolecular therapeutics from entering the brain make it a tricky problem for treating PD. Herein, we fabricated multi-functionalized LNP loaded with Exe to reduce the production of α-synuclein and effectively treat PD. CSO made it possible for LNP to release Exe responsively at focal cells. With both targeting and increasing BBB permeability functions at one time, intracerebral delivery of Exe was greatly enhanced.

2. Materials and methods

2.1. Materials

1,2-dimyristoyl-rac-glycero-3-methoxypolyethylene glycol-2000 (DMG-PEG2000) and lecithin (Lec) was purchased from Aladdin chemical reagent company (Shanghai, China). L-α-lysophosphatidylcholine (Lpc), cholesterol and stearic acid (SA) were purchased from Sigma-Aldrich (St. Louis, MO, USA). Borneol was purchased from Selleck Chemicals (Shanghai, China). Exenatide (Exe) was purchased from MedChemExpress (Monmouth Junction, NJ, USA). Dir, Did, and DiI were purchased from Yeasen Co. Ltd (Shanghai, China). Ultrafiltration centrifuge tube (MWCO = 100 kDa) was purchased from Merck Millipore (Darmstadt, Germany). Chitosan (CSO), degraded using chitosanase in our laboratory (Mw = 18 kDa), was utilized. Tyrosine hydroxylase (TH) antibodies were purchased from Cell Signaling Technology Co.Ltd (Danvers, MA, USA). The commercial enzyme-linked immunosorbent assay (ELISA) kits of dopamine and GDNF were purchased from Elabscience Biotechnology Co., Ltd (Wuhan, China). 1-Methyl-4-phenyl-1,2,3,6-tetrahydropyridine hydrochloride (MPTP) was purchased

from Aladdin chemical reagent company (Shanghai, China) and used to induce PD model in C57BL/6 mice. α-synuclein antibody, GSK-3β antibody, NF-κB antibody, claudin-5 antibody and TNF-α antibodies were purchased from Abcam (Boston, USA).

2.2. Cell lines and animals

The bEnd.3 cell (brain-derived endothelial cells. 3, which can be used in BBB model studies) and SH-SY5Y cell (a human neuroblastoma cell line with TH activity is used to study neuronal function, including PD) were purchased from Chinese Academy of Sciences Shanghai Cell Bank. C57BL/6 mice (aged 15 months, male, 32–36 g) were purchased from Shanghai Slack Laboratory Animal Co., Ltd. Animals were raised in a pathogen-free environment with a 12 h light/dark cycle at 25 ± 3 °C and had *ad libitum* access to food and water. Animal handling protocols and experiments were approved by Zhejiang University Laboratory Animal Ethics Committee.

2.3. Measurement of TEER of bEnd.3 cells

bEnd.3 cells (5×10^5 per cell) were seeded on the upper chamber of transwell plate (12 wells, pore size of 4 μm, polyester membrane) for two weeks to form physiological BBB. Transepithelial electrical resistance (TEER, $\Omega \cdot cm^2$) of the physiological BBB was measured by a transmembrane resistance meter (RS1203, Metalworking Hongtai, China). Borneol (10 μg/ml) was incubated with the cells for 0.5, 1, 4 and 6 h and the TEER was measured, respectively.

2.4. Western blot

bEnd.3 cells were seeded in 6-well cell culture plates at a cell density of 3×10^5 cells/well and cultured at 37 °C, 5% CO_2 for 1 week in cell culture incubator (3110, Thermo Forma, USA) to form dense TJs. Borneol was added (10 μg/ml) and incubated for 8 h. Cells were scraped, and RIPA cell lysate was added to lyse the cells for 30 min. Cell debris was centrifuged at 4 °C, 12,000 rpm for 20 min by Ultracentrifuge (Allegra ^{TM} 64R, Beckman, USA). Total protein concentration was detected with BCA protein assay kit. The protein solution was denatured by boiling at 100 °C for 15 min, actin was used as an internal reference protein, and the expression of the target protein CLDN-5 was detected by electrophoresis (PowerPac^{TM} Basic, BioRad, USA).

Cytoplasmic protein extraction: bEnd.3 cells were seeded in 6-well cell culture plates at a cell density of 3×10^5 cells/well and cultured at 37 °C, 5% CO_2 for 1 week. Borneol was added (10 μg/ml) and incubated for 8 h. Cells were washed with PBS and collected by centrifugation. The supernatant was discarded. 200 μl of PMSF-added cytoplasmic protein extraction reagent A was added. Cell pellet was vortexed vigorously for 5 s to completely suspend and disperse the cell pellet. 10 μl cytoplasmic protein extraction reagent B was added. Cells were vortexed vigorously for 5 s and centrifuged at 12,000–16,000 g for 5 min at 4 °C. The supernatant was immediately drawn into a pre-cooled plastic tube, which was the extracted cytoplasmic protein.

2.5. Immunofluorescence of borneol translocating claudin-5 into the cytoplasm

bEnd.3 cells were seeded on the cell culture plate for 1 week to form physiological BBB. Borneol (10 μg/ml) was incubated with the cells for 1 h. After being fixed with 4% paraformaldehyde, cell membranes were incubated with claudin-5 antibody and labeled with Dil. Confocal laser scanning microscope (CLSM, Olympus Ix81-FV1000, Japan) was used to observe the expression and relative position of CLDN-5.

2.6. Synthesis of borneol-modified SA

SA (1.5 g, 5.25 mmol) was dissolved in 15 ml anhydrous dichloromethane (DCM). Then, a catalytic amount of dimethylformamide was added dropwise. The reaction system was placed in an ice bath, followed by addition of oxalyl chloride (890 μl, 10.43 mmol). The mixture was stirred (1,500 rpm) in an ice bath for 1 h, followed by being stirred at room temperature for 6 h. The reaction liquid was evaporated by rotary evaporator (IKA RV10, Germany) to remove the solvent. Borneol (0.5 g, 3.24 mmol) was dissolved in anhydrous DCM followed by the addition of 4-dimethylaminopyridine (51.9 mg, 0.42 mmol) and triethylamine. The mixture was added to acid chloride synthesized above and stirred (1,500 rpm) at 0 °C for 1 h, followed by 12 h at room temperature. The solvent was removed by vacuum drying. The reaction was quenched with saturated ammonium chloride, extracted with ethyl acetate and washed with saturated sodium carbonate. The organic layer was dehydrated with anhydrous sodium sulfate. The solvent was removed, and the crude product was obtained.

The crude product was purified by silica gel column chromatography with petroleum ether: ethyl acetate = 100:1, 80:1 and 60:1 as eluent. Finally, borneol-stearic acid (Bo-SA) was obtained, and its structure was confirmed by nuclear magnetic resonance (NMR, Avance III 500 M, Bruker, Switzerland) using $CDCl_3$ as solvent.

2.7. Fabrication of multi-functionalized LNP

LNP were fabricated with solvent diffusion method. DMG-PEG2000 served as the skeleton of LNP, and PEG modification could avoid being engulfed by the reticuloendothelial system. Cholesterol was used to maintain the rigidity of the nanoparticles and improve the loading efficiency. Lpc is the specific substrate of Mfsd2a and was used to target the BBB. Bo-SA was used to increase the permeability of BBB. Briefly, DMG-PEG2000, Lpc, cholesterol and BoSA were dissolved in ethanol (of which the concentration was 20 mg/ml) at 60 °C with a mass ratio of 25:20:32:40. CSO aqueous solution (1.6 mg/ml) was mixed with the above lipid solution (v: $v = 5{:}95$) and the mixture was resuspended in water (10 ml) on magnetic stirrer (DF-101S, Gongyi Yuhua Instrument, China). Suspension was stirred at 25 °C, 1,500 rpm for 0.5 h. These nanoparticles could both target and increase BBB permeability and release drugs in an environment-responsive manner, abbreviated as Lpc-BoSA/CSO.

DMG-PEG2000, Lpc, cholesterol and BoSA were dissolved in ethanol (of which the concentration was 20 mg/ml) at 60 °C

with mass ratio of 25:20:32:40. CSO (1.6 mg/ml) and Exe (molar ratio = 2:1, 1:1, 1:2, 1:5) aqueous solutions were mixed. The above aqueous solution was mixed with the lipid mixture (5:95, v/v), and then dispersed in deionized water to obtain Lpc-BoSA/CSO-Exe.

Nanoparticles with BBB targeting and increasing permeability functions were DMG-PEG2000:Lpc:cholesterol: BoSA = 25:20:32:40, which was abbreviated as Lpc-BoSA. Exe aqueous solution (50 mg/ml) was mixed with the lipid mixture (5:95, v/v), and then dispersed in deionized water to obtain Lpc-BoSA/Exe. The following drug-loaded nanoparticles were prepared in the same way. Nanoparticles targeting BBB function were DMG-PEG2000:Lpc:cholesterol:SA = 25:20:32:40, which was abbreviated as Lpc-SA. Nanoparticles with BBB increasing permeability function were DMG-PEG2000:Lec: cholesterol:BoSA = 25:20:32:40, which was abbreviated as Lec-BoSA. Regular nanoparticles were DMG-PEG2000:Lec: cholesterol:SA = 25:20:32:40, which was abbreviated as Lec-SA.

The particle size and zeta potential of the above nanoparticles were measured by dynamic light scattering (Anton Paar Litesizer 500, Austria).

2.8. Measurement of encapsulation efficiency and drug loading efficiency

Drug-loaded nanoparticles were prepared as mentioned in Section 2.7. Drug-loaded nanoparticles were put in the inner tube of an ultrafiltration centrifuge tube (MWCO = 100 kDa), and were centrifuged at 5000 rpm (TDL-40C, Shanghai Anting Scientific Instrument, China) for 20 min. The concentration of Exe in the outer tube was detected with a high-performance liquid chromatography (HPLC, Agillent 1200, USA) instrument. The HPLC mobile phase of Exe was 0.1% TFA in acetonitrile: 0.1% TFA in water = 20%: 80%, UV = 220 nm. Encapsulation efficiency (EE%) and drug loading efficiency (DL%) were calculated according to Eqs. (1) and (2).

$$DL\% = (M_{Exe} - C \times V)/(M_{Exe} + M_{LNP}) \times 100 \quad (1)$$

$$EE\% = (M_{Exe} - C \times V)/M_{Exe} \times 100 \quad (2)$$

Where M_{Exe} is the total amount of Exe, C is Exe concentration in outer tube, V is the volume in the outer tube, and M_{LNP} is the weight of blank LNP.

2.9. Hemolysis of LNP

Blood (3 ml) was placed in a vacuum blood collection tube (coated with anticoagulant). Blood was centrifuged at 500 g for 5 min, and plasma was discarded. The blood was filled with 150 mM NaCl solution to the original plasma level and centrifuged at 500 g for 5 min. Above steps were repeated to wash the blood cells. Finally, the supernatant was discarded, replaced with pH 7.4 PBS and mixed gently. The erythrocytes obtained above were diluted 50-fold with pH 7.4 PBS. Five LNP of which the final concentration was 0.5 mg/ml, 0.25 mg/ml and 0.125 mg/ml were incubated with diluted erythrocytes at 37 °C for 1 h in a water bath with a constant temperature oscillator (HZ-8812S-B, Changzhou Kaihang Instrument, China). 20% Triton X-100 was added as positive control and PBS as negative control. Finally, the erythrocyte and nanoparticle mixture were centrifuged at 500 g for 5 min to pellet intact erythrocytes. The supernatant was measured with a microplate reader at 400–541 nm (Model 680, Bio-Rad, USA). Higher Lpc content will lead to an increase in the hemolysis rate of LNP. We did preliminary content screening in the early stage to control the hemolysis rate below 5%.

2.10. Detection of intracellular microenvironment in PD cell model

SH-SY5Y cells were seeded in 24-well plates and damaged with 3 mM MPP^+ (1-methyl-4-phenylpyridinium iodide) to induce a PD cell model. Cells were washed with PBS, followed by co-incubation with 6 μM BCECF-AM for 30 min at 37 °C in 5% CO_2. Cells were washed with pre-warmed PBS and observed by CLSM.

2.11. Sensitive release of multi-functionalized LNP with FRET effect

Lpc-BoSA/CSO and Lpc-BoSA were loaded with Dil-DiO (=1:1, w/w). SH-SY5Y cells damaged by MPP^+ were seeded in a 24-well plate with a glass disc at the bottom. Equal amounts of nanoparticles were added, and after 2 h uptake, the culture medium was replaced with fresh culture medium for another 0.5, 2 and 4 h. Cells were fixed with 4% paraformaldehyde for CLSM observation. Images were acquired with 488 nm excitation, 490–505 nm spectral filter for DiO detection and 535–635 nm spectral filter for DiI detection. Fluorescence resonance energy transfer (FRET) energy transfer efficiency was calculated according to following formula: $E = I_{Dil} / (I_{Dil} + I_{DiO})$, where I_{Dil} was the acceptor fluorescence intensity, and I_{DiO} was the donor fluorescence intensity.

2.12. Release of Exe in vitro

Lpc-BoSA/CSO-Exe, Lpc-BoSA/Exe, Lpc-SA/Exe, Lec-BoSA/Exe, and Lec-SA/Exe were put in ultrafiltration centrifuge tube (50 ml, MWCO = 100 kDa) against 25 ml acid buffer (pH 6.2 acetic acid and sodium acetate). Meanwhile, Lpc-BoSA/CSO-Exe was put in ultrafiltration centrifuge tube (50 ml, MWCO = 100 kDa) against 25 ml pH 7.4 PBS. Ultrafiltration centrifuge tubes were put in the shaker at 37 °C, 100 rpm. Sampling at 0, 2, 6, 20, 26, 36, and 48 h for released Exe and an equal volume of release medium (25 ml) was added. Exe content was detected by HPLC. The HPLC mobile phase for Exe was 0.1% TFA in acetonitrile: 0.1% TFA in water = 20%: 80%, UV = 220 nm.

2.13. Cytotoxicity of LNP

bEnd.3 cells and SH-SY5Y cells were seeded in 96-well plates at a cell density of 1×10^4/well and 0.6×10^4/well, respectively, and cultured at 37 °C in 5% CO_2. When the cell confluence reached 75%, different concentrations (0, 50, 100 and 300 μg/ml) of Lpc-BoSA/CSO, Lpc-BoSA, Lpc-SA, Lec-BoSA,

and Lec-SA were added. 24 h later, 20 μl of 5.0 mg/ml MTT solution was added to each well. 4 h later, the medium was discarded and 200 μl of DMSO was added. The plates were put in a shaker at 37 °C for 30 min and the absorbance at 570 nm was detected with a microplate reader.

2.14. Lysosomal escape of multi-functionalized LNP

Lpc-BoSA/CSO and Lpc-BoSA were labeled with 1% (w/w) Dil and stirred (1,500 rpm) at room temperature for 1 h. They were dialyzed (MWCO = 3.5 kDa) for 24 h to remove free Dil. SH-SY5Y cells were seeded on small dishes and incubated at 37 °C in 5% CO_2. Dil-labeled Lpc-BoSA/CSO and Lpc-BoSA were incubated with SH-SY5Y cells for 24 h. Then, Lysotracker was added. The co-localization of LNP and lysosomes was observed by CLSM.

2.15. Cellular uptake and in vitro BBB targeting

The BBB physiological cell model was constructed. bEnd.3 cells were grown in the upper chamber of the transwell and SH-SY5Y cells in the lower. The Dil-labeled Lpc-BoSA/CSO and Lec-SA were added to the insert and incubated with cells for 2, 4 and 8 h, respectively. After that, cells were washed with cold PBS, followed by 30-min fixation with 4% formaldehyde. Nucleus were stained with Hoechst 33342 and cells were imaged using CLSM. bEnd.3 cells were seeded in 6-well plates (3×10^5 per well). After co-incubation with Dil-labeled nanoparticles for 4 h, cells were trypsinized. Cell suspension was collected and centrifuged at 1,000 rpm for 5 min. The culture medium was discarded, and cells were resuspended in PBS. The uptake of nanoparticles by bEnd.3 cells was measured by flow cytometry (CytoFLEX S, Beckman Coulter, USA).

2.16. Internalization pathways of multi-functionalized LNP

Different inhibitors were used to study the internalization pathways of LNP. Briefly, chlorpromazine (CPZ, 30 μM), filipin (10 μM) and amiloride (100 μM) were preincubated with SH-SY5Y cells for 30 min. After that, cells were incubated with Dil-labeled Lpc-BoSA/CSO for 4 h, followed by 4% paraformaldehyde fixation and observation by CLSM.

2.17. In vitro pharmacodynamics study of LNP to repair dopamine neurons

In vitro physiological BBB model was constructed. SH-SY5Y cells damaged by 3 mM MPP^+ were seeded on the slide in the lower chamber and co-cultured with bEnd.3 to establish *in vitro* PD model. Lpc-BoSA/CSO-Exe, Lpc-BoSA/Exe, Lpc-SA/Exe, Lec-BoSA/Exe, Lec-SA/Exe and Exe were added to the insert of which the concentration of Exe was 150 nM. SH-SY5Y cells in control group were not damaged and simulated physical condition. PBS was added to PD group as negative group. 48 h later, SH-SY5Y cells on the slide were collected to detect the expression of TH through immunofluorescence.

2.18. In vivo distribution of LNP

Dir-labeled LNP were intravenously administered into C57BL/6 mice via tail vein by injector (YLS-Q9G, Jinan Yiyan Technology, China). 4 h later, mice were perfused with PBS and executed. Brains were collected for *ex vivo* imaging using the *in vivo* imaging system (IVIS, CRI Inc., Woburn, US) at excitation and emission wavelengths of 704 and 745 nm.

2.19. LNP crossed the BBB into the brain parenchyma

Dil-labeled LNP were intravenously administered into C57BL/6 mice. 4 h later, mice were perfused with PBS and fixed with 4% paraformaldehyde. Brains were cut into thin slices with a cryostat (Leica UC7, Germany). Cerebral blood vessels were labeled with CD31 antibody. The amount of LNP across cerebral blood vessels into the brain parenchyma was observed by fluorescence microscope (Zessi Observer Z1, Germany).

2.20. Open-field test

Mice were put in a 45 cm × 45 cm × 45 cm acrylic cube after being handled to eliminate anxiety and tension. Each animal was permitted to explore at will for 10 min. Total distance, time immobile, center zone time and center zone entries were recorded during the 10-min test by ANY-maze system (ViewPoint, France).

2.21. Rotarod test

Mice were positioned on a rotarod. Two evaluation methods were tested, including rotating at a fixed 15 rpm speed and accelerating rotating from 4 to 40 rpm in 100 s. The time during which each mouse remained on the rod was recorded by rotarod (Panlab, USA).

2.22. Pole test

Mice were positioned head up atop a vertical pole that had a rough surface (70 cm tall, 1 cm diameter). The times required for the mice to turn around (t-turn) and climb to the bottom of the pole (t-total) were recorded.

2.23. TH, dopamine, α-synuclein, GSK-3β and AKT expression detection

After drug administration, mice were perfused with pH 7.4 PBS, and the brains were removed, fixed in 4% paraformaldehyde for 48 h, and embedded in paraffin. Slices of striatum (Cpu) and substantia nigra pars compacta (SNpc) were taken with a tissue slide microtome (Leica SM2010R, Germany), and the expression of TH, α-synuclein, GSK-3β and AKT were detected by immunohistochemical method. Fresh brain tissue slices of the striatum (Cpu) and substantia nigra pars compacta (SNpc), with a thickness of 200 μm, were taken by a cryostat (NX70, Thermo, USA), and were used to detect the expression of dopamine (DA) by Elisa kit.

2.24. Lewy body detection

Mouse brain tissues were dewaxed, Congo red stained and dehydrated, sealed with neutral gum, and observed for the deposition of Lewy bodies under Olympus microscope (bx63, Olympus, Japan).

2.25. Health monitoring for possible severe side effects in vivo

During drug administration, body weight of mice was monitored. Blood glucose was monitored with a glucometer (HGM-112, Suzhou Erda Medical Equipment, China) and glucose test strips before, during and after drug administration.

2.26. Statistics

For statistical analysis, data were subjected to student's *t*-tests with GraphPad Prism8.0 to determine differences. *P* values of less than 0.05 were accepted as statistically significant.

3. Results and discussion

3.1. Borneol increased BBB permeability by translocating TJ proteins into the cytoplasm

Borneol increased BBB permeability by reducing TEER. As shown in Fig. 1A, TEER was the lowest ($P < 0.001$), below 150 Ω•cm^2, 1 h after borneol treatment. TEER is an indicator of cell barrier permeability. Decreased TEER indicates increased barrier permeability. TJs are an important component of the BBB in exerting its barrier properties. Therefore, we examined the expression of claudin-5 (CLDN-5), one of the TJs of BBB, which is a protective barrier to prevent most substance from entering the brain. As shown in Fig. 1B, the total amount of CLDN-5 remained unchanged before and after borneol treatment. The cytoplasm of bEnd.3 cells was extracted by cytoplasm extraction kit and the content of CLDN-5 was detected. Results showed the content of CLDN-5 in borneol group was significantly higher than that in control group (Fig. 1C and 1D, $P < 0.05$), which suggested borneol translocated CLDN-5 into the cytoplasm. Immunofluorescence results confirmed that CLDN-5 was significantly translocated into the cytoplasm 1 h after borneol treatment (white arrows indicated proteins translocating into the cytoplasm) (Fig. 1E). These experiments indicated that borneol increased BBB permeability by translocating CLDN-5 to the cytoplasm.

3.2. Fabrication of multi-functionalized LNP

Fig. 2A depicts the reaction of borneol and steric acid to form an ester. In the ^{1}H NMR spectrum, H at δ 4.87 ppm was the hydrogen proton on the six-carbon ring adjacent to the ester group. H at about δ 0.8 ppm was the methyl protons on borneol and SA. H at about δ 1.2 ppm was the methylene protons of the six-carbon ring and the long carbon chain on SA. The protons at δ 1.6–2.4 ppm were hydrogen protons near the ester group.

The solvent diffusion method was used to fabricate LNP. Lpc, as one of the components of LNP was used to target the brain. Non-targeted phospholipids were replaced with Lec. Borneol (Bo), acting as a messenger molecule to increase BBB permeability, was chemically linked to SA. CSO achieved environment-responsive drug release through proton sponge effect. Briefly, Lpc-BoSA/CSO could enter the brain parenchyma via transcellular transcytosis and paracellular pathways (Fig. 2B). Fig. 2C shows morphological structures of LNP under transmission electron microscope

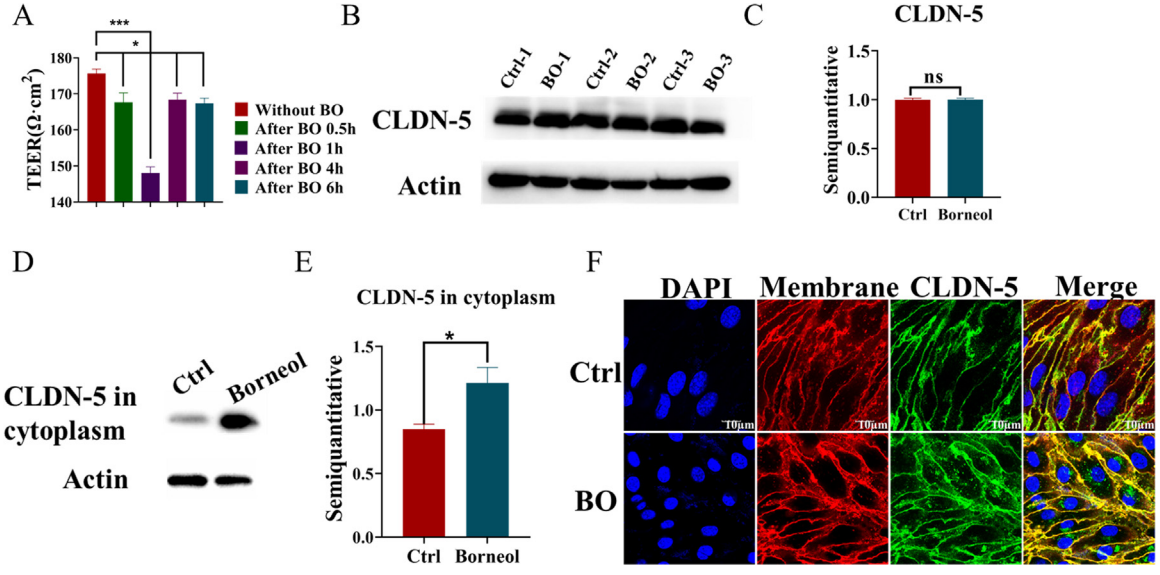

Fig. 1 – Borneol increased BBB permeability by translocating CLDN-5 into the cytoplasm. (A) The timeliness of borneol-mediated reduction in the TEER of bEnd.3 cells. (B) The total content of CLDN-5 did not change after borneol treatment. On the right was the semiquantitative result. (C) Western blot images of CLDN-5 translocating into the cytoplasm after borneol treatment. (D) Semiquantitative results of (C). (E) Immunofluorescence image of CLDN-5 translocating into the cytoplasm after borneol treatment (Scale bar: 10 μm). ($n = 3$, *$P < 0.05$ and ***$P < 0.001$).

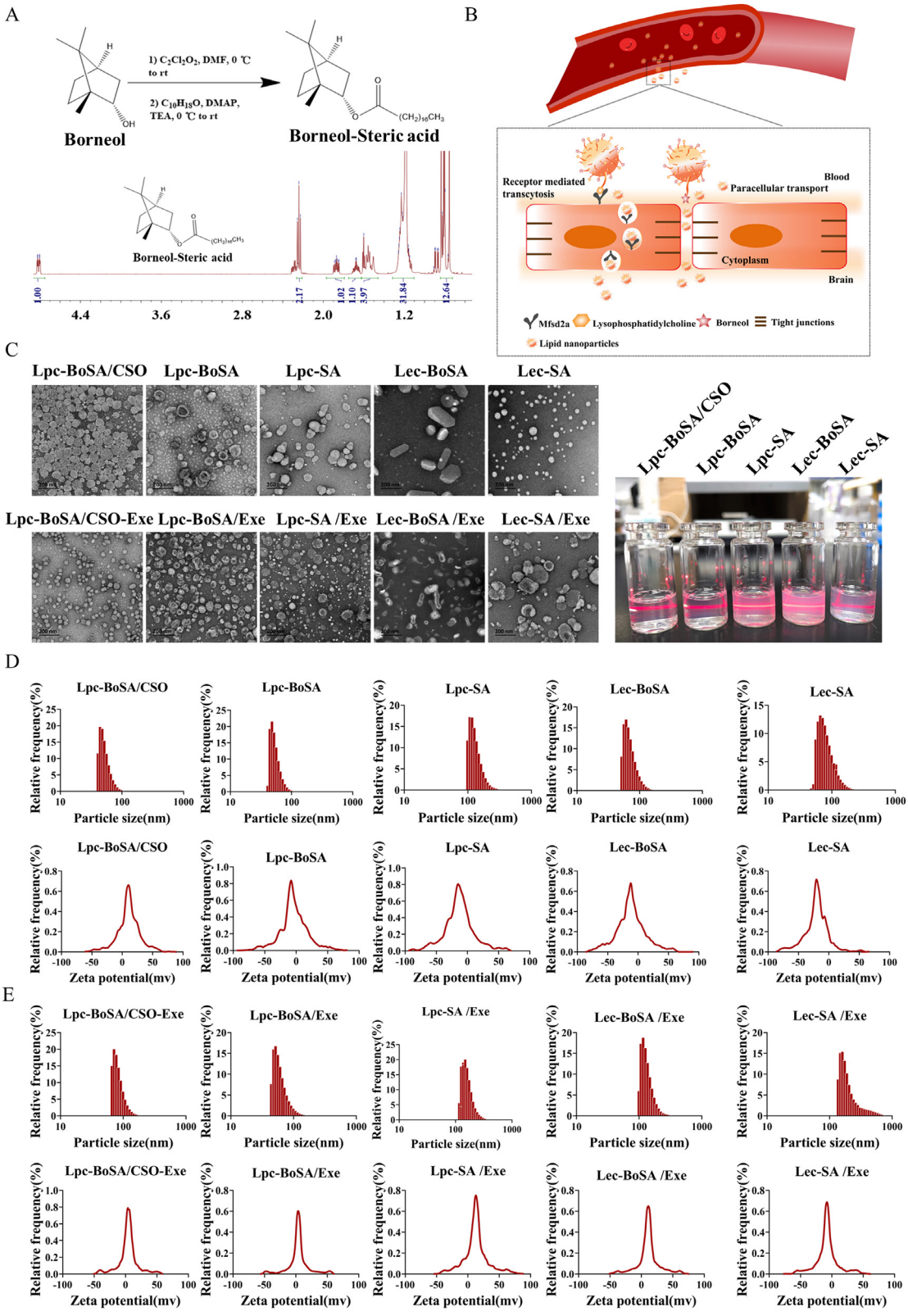

Fig. 2 – Fabrication and physicochemical properties evaluation of functionalized LNP. (A) Reaction of borneol with SA to synthesize ester and the ^{1}H NMR spectrum of the synthesized ester; (B) Schematic diagram of the pathways that functionalized LNP crossed the BBB into the brain parenchyma: (1) transcytosis mediated by the highly expressed Mfsd2a receptor on brain microvascular endothelial cells, (2) paracellular pathway between endothelial cells via increased BBB permeability by borneol; (C) TEM images of LNP and drug-loaded nanoparticles (scale bar: 200 nm), on the right is the LNP (1 mg/ml) illuminated by a laser pointer; (D) Particle size and zeta potential distribution of LNP and (E) drug-loaded nanoparticles.

(TEM). Lpc-BoSA/CSO had a unique structure, which might endow it with long circulation *in vivo* and not being easily phagocytosed by the reticuloendothelial system [42]. The particle size was 78.7 ± 0.79 nm, and zeta potential was 7.9 ± 1.24 mV. Lpc-BoSA had a vesicle-like structure and its particle size and zeta potential were 78.5 ± 4.51 nm and -6.9 ± 1.15 mV, respectively. Lpc-SA had spherical-like shape and its particle size and zeta potential were 171.9 ± 1.60 nm and −17.6 ± 1.24 mV, respectively. Lec-BoSA had a rod-like structure and its particle size and zeta potential were 139.1 ± 9.58 nm and −18.3 ± 2.38 mV, respectively. Lec-SA had a spherical shape and its particle size and zeta potential were 194.0 ± 10.74 nm and −22.2 ± 0.43 mV, respectively (Fig. 2D). As shown in Fig. 2C (right), these nanoparticles dispersed uniformly in the water.

When CSO:Exe = 2:1, 1:1, 1:2 (molar ratio), the preparation was unstable and had turbidity. The CSO:Exe = 1: 5 formula was preferred to obtain a better preparation form, which might be related to the capacity of hydrophilic CSO molecules to embed into LNP to form nanoparticles. So CSO:Exe = 1: 5 (molar ratio) was selected. The TEM of the drug-loaded nanoparticles is shown in Fig. 2C, and the particle size and zeta potential are shown in Fig. 2E.

Borneol is a highly lipid-soluble bicyclic terpene molecule, for which its administration route is mostly gavage. The doses of natural and synthetic borneol recommended for clinical use are 0.3–0.9 g and 0.15–0.3 g, respectively [43]. Herein, we have been able to increase the concentration of borneol in the blood through intravenous injection by chemically linking borneol onto LNP. In this way, the dosage of borneol is reduced and the convenience of drug administration is increased.

CSO is an alkaline hydrophilic polymer with good biocompatibility and degradability. The pKa of the amino group in CSO is 6.5. In a medium with a pH of 6.5 or so, swelling occurs due to the protonation of the amino group, resulting in a large osmotic pressure, which is beneficial to drug release. It is often used in the construction of pH-responsive nanocarriers. PD lesion site usually presents a weakly acidic environment due to pathological factors such as inflammation, hypoxia, and ROS [44].

3.3. *Hemolysis risk assessment, encapsulation efficiency and in vitro release studies of functional LNP*

The hemolysis test detected the hemolysis risk of nanoparticles *in vivo*, which reflected the *in vivo* safety of the nanoparticles when administered intravenously. As shown in Fig. 3A and 3B, the hemolysis rate of all LNP was less than 5% at the concentration of 0.5 mg/ml. EE% and DL% of LNP for Exe are shown in Table 1.

LNP (final concentrations were 0, 50, 100 and 300 μg/ml) were incubated with bEnd.3 cells and SH-SY5Y cells respectively. Cell viability was detected by MTT assay. As shown in Fig. 3C, when the nanoparticle concentration was 300 μg/ml, cell viability was still more than 80%, suggesting the LNP were safe.

The stability test results of Lpc-BoSA/CSO are shown in Fig. 3D. The particle size was maintained at about 90 nm at 25 °C and 55% humidity for six consecutive days, indicating good stability.

Literature shows that PD lesions have high levels of oxidative stress, and H_2O_2 levels are increased significantly [44,45]. Such microenvironment makes it easy for Lpc-BoSA/CSO to release Exe through proton sponge effect. We used a slightly acidic buffer to simulate the *in vivo* focal microenvironment and the release of each formulation was shown in Fig. 3E. Lpc-BoSA/CSO in pH 7.4 PBS was used as

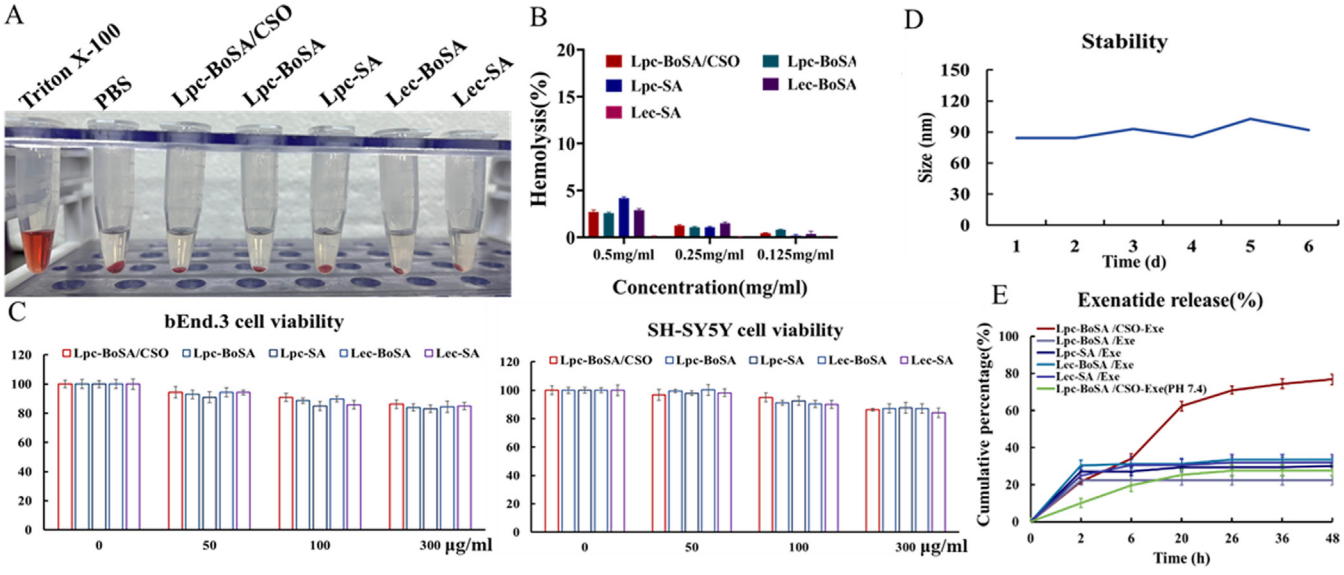

Fig. 3 – Functional evaluation of LNP. (A) Hemolysis risk assessment of LNP; (B) Hemolysis rate of LNP at 0.5 mg/ml, 0.25 mg/ml and 0.125 mg/ml ($n = 3$); (C) Cytotoxicity evaluation of LNP on bEnd.3 cells and SH-SY5Y cells ($n = 6$); (D) Stability assessment of Lpc-BoSA/CSO; (E) Exe release from LNP *in vitro* in acid buffer and pH 7.4 PBS ($n = 3$).

Table 1 – EE% and DL% of LNP.

	Lpc-BoSA/CSO	Lpc-BoSA	Lpc-SA	Lec-BoSA	Lec-SA
EE%	56.0% ± 1.10%	63.2% ± 3.45%	60.0% ± 2.30%	49.6% ± 3.20%	48.0% ± 2.19%
DL%	10.2% ± 1.40%	11.5% ± 1.00%	10.9% ± 1.20%	9.03% ± 1.70%	8.74% ± 2.50%

a control. The release of Exe from Lpc-BoSA/CSO in acidic buffer was 76.70% and less than 40% in other LNP. The release of Exe from Lpc-BoSA/CSO in pH 7.4 PBS was less than 40%, suggesting that Lpc-BoSA/CSO achieved responsive release, which might be related to the proton sponge pump effect.

3.4. *Responsive release and lysosomal escape of functional LNP*

Responsive release of the drug was confirmed by FRET. When the fluorescence pair Dil-DiO were in close proximity, non-radioactive energy transfer occurred, and Dil was excited. When the fluorescent pair were released and the distance increased, the Dil fluorescence decreased or disappeared. As shown in Fig. 4A, Lpc-BoSA did not release the fluorescent pair, so Dil was continuously excited. Lpc-BoSA/CSO released fluorescence pairs, which decreased the Dil fluorescence. Energy transfer efficiency is shown in Fig. 4B.

TEM images of LNP before, during and after release in a slightly acidic environment (pH 6.2 acetic acid and sodium acetate) are shown in Fig. 4C. Under pH 7.4 circumstances, Lpc-BoSA/CSO had a complete shape and uniform particle size. After being placed in a slightly acidic environment with pH 6.2 for 2 h, the nanoparticles gradually disintegrated and the particle sizes varied. After 4 h, the nanoparticles completely disintegrated, which showed that Lpc-BoSA/CSO had an acid-responsive release function. We measured intracellular pH of PD cell model (SH-SY5Y cells damaged by MPP^+). PH-sensitive microfluorometry probe BCECF-AM indicated that PD cells tended to have a more acid microenvironment than control ($P < 0.05$), which was the environmental condition for Lpc-BoSA/CSO to release responsively (Fig. 4D).

We investigated the lysosomal escape capacity of Lpc-BoSA/CSO and Lpc-BoSA. The results were shown in Fig. 4E, green Lpc-BoSA/CSO did not co-localize with red lysosomes and was mainly distributed in the cytoplasm, while Lpc-BoSA mainly co-localized with lysosomes, indicating that Lpc-BoSA/CSO had lysosome escaping function. There is a significant difference in the Pearson's R between Lpc-BoSA/CSO and Lpc-BoSA ($P < 0.05$).

3.5. *Multi-functionalized LNP crossed the BBB, rescuing SH-SY5Y cells*

The target destination of lipid nanoparticle-encapsulated Exe was dopaminergic neuron cells in the brain parenchyma. Unlike conventional cellular uptake experiments, we did not co-incubate LNP with bEnd.3 and SH-SY5Y cells separately to observe the cell uptake. Instead, *in vitro* BBB model was constructed, and bEnd.3 cells were seeded in the

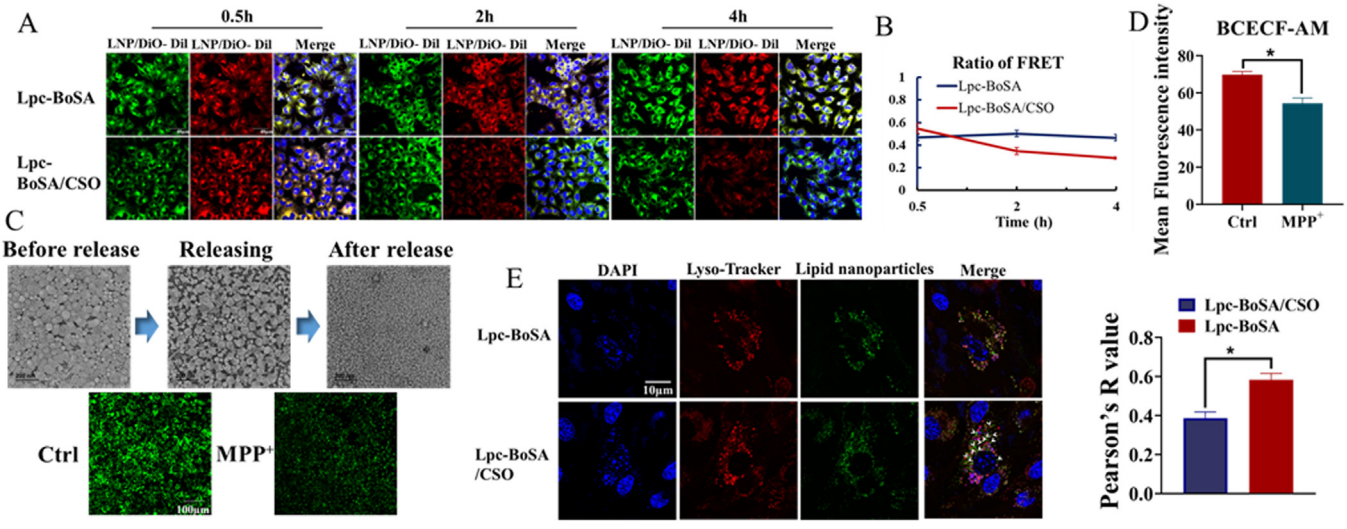

Fig. 4 – Responsive release and lysosomal escape evaluations of Lpc-BoSA/CSO. (A) FRET effect of Lpc-BoSA/CSO; (B) Energy transfer efficiency of (A) ($n = 3$); (C) TEM images of Lpc-BoSA/CSO before, during and after release in acid buffer (scale bar: 200 nm). Distribution of the pH-sensitive microfluorometry probe BCECF-AM in normal SH-SY5Y cells (Ctrl) and MPP^+ damaged SH-SY5Y cells (scale bar: 100 μm); (D) Semi-quantification of fluorescence intensity in Fig. 4C; (E) Immunofluorescence images of lysosomal escape of Lpc-BoSA/CSO (scale bar: 10 μm), on the right is the Pearson's coefficient for co-localization of lysosome and Lpc-BoSA/CSO ($n = 3$, $^*P < 0.05$).

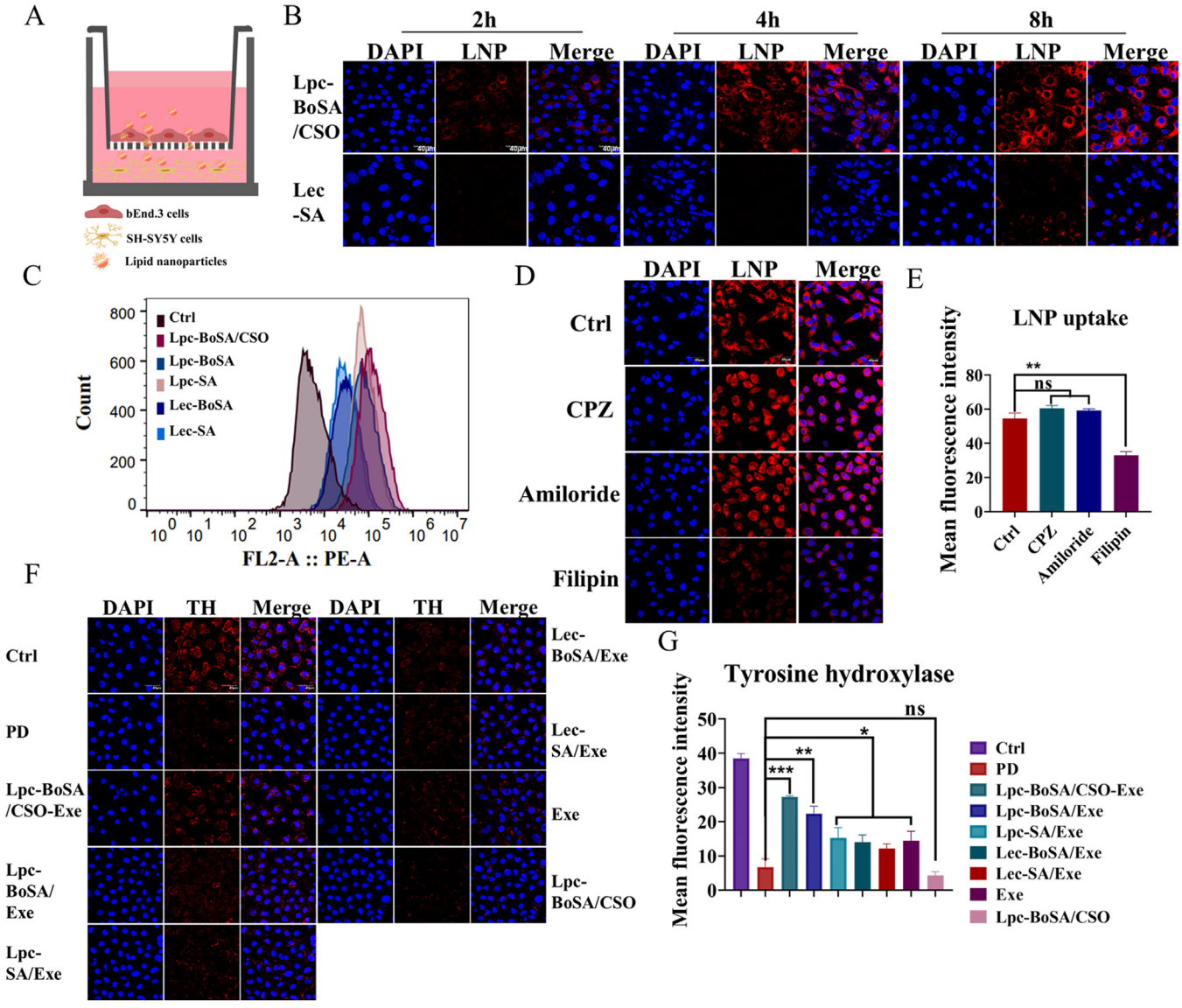

Fig. 5 – Cellular uptake, mechanism, and pharmacodynamics of LNP. (A) Co-culture of bEnd.3 cells and SH-SY5Y cells to simulate *in vitro* PD model; (B) *In vitro* BBB permeability-increasing and targeting ability of LNP at 2, 4, 8 h (scale bar: 40 μm); (C) Flow cytometry of bEnd.3 uptake of LNP; (D) Different inhibitors were used to investigate the mechanism of cellular uptake of LNP; (E) Fluorescence semi-quantification of Fig. 5D ($n = 3$, $^{**}P < 0.01$); (F) Cellular pharmacodynamics of LNP reflected by TH expression of SH-SY5Y cells (scale bar: 40 μm); (G) Semiquantitative results of Fig. 5F ($n = 3$, $^{*}P < 0.05$, $^{**}P < 0.01$, $^{***}P < 0.001$).

upper chamber of the transwell and SH-SY5Y cells in the lower chamber (Fig. 5A). Dil-labeled nanoparticles were added to the insert and incubated for 2, 4, and 8 h, respectively. As shown in Fig. 5B, Lpc-BoSA/CSO had BBB-targeting and permeability-increasing functions, so they could cross into the lower compartment through receptor-mediated transcytosis and paracellular pathway. Therefore, the uptake of Lpc-BoSA/CSO by SH-SY5Y cells was remarkably more than Lec-SA. Fluorescence signal of Lpc-BoSA/CSO reached the maximum at 4 h and remained unchanged at 8 h.

Flow cytometry results showed that bEnd.3 cells had more uptake of Lpc-modified Lpc-BoSA/CSO, Lpc-BoSA and Lpc-SA and less uptake of Lec-BoSA and Lec-SA (Fig. 5C), which might be due to the fact that Lpc can be taken up through transcytosis mediated by Mfsd2a receptor on bEnd.3 cells.

There are many internalization pathways of nanoparticles, including clathrin-mediated endocytosis, caveolin-mediated endocytosis and macropinocytosis. Several specific endocytic inhibitors were used to identify the internalization pathways of functionalized LNP. Chlorpromazine (CPZ, clathrin-mediated endocytosis) and amiloride (macropinocytosis) did not affect the uptake of nanoparticles by SH-SY5Y. However, uptake was significantly reduced after cells were treated with filipin (caveolin-mediated endocytosis), down to 60.56% of that in the control group ($P < 0.01$), suggesting that

the uptake of nanoparticles was mainly caveolin-mediated endocytosis (Fig. 5D and 5E).

In vitro PD model was constructed. Functionalized LNP transported across the BBB into the lower compartment via transcytosis and paracellular pathway via increased permeability by borneol. Exe restored injured SH-SY5Y cells and increased the expression of TH. As shown in Fig. 5F, with functions of BBB targeting, permeability-increasing and Exe responsive release, Lpc-BoSA/CSO-Exe entered the lower chamber and Exe was released extensively. The expression of TH in Lpc-BoSA/CSO-Exe group was the largest, being 4.01 times of that in PD group ($P < 0.001$), which indicated that Lpc-BoSA/CSO significantly enhanced the efficacy of Exe (Fig. 5G).

3.6. *Multi-functionalized LNP targeted and entered the brain in vivo*

The presence of BBB makes it difficult for most therapeutics to enter the brain parenchyma. Functionalized LNP entered into the brain in a two-pronged approach, namely transcytosis and paracellular pathways, allowing more nanoparticles to enter the brain. Lpc-BoSA/CSO and Lpc-BoSA had both BBB targeting and permeability-increasing functions and *in vivo* imaging system showed they had the brightest signal in the brain (Fig. 6C), which suggested nanoparticles entered the brain in large quantities. The distribution of Lpc-BoSA/CSO in other organs throughout the body is shown in the lower panel of Fig. 6C.

To intuitively observe the entry of LNP into brain parenchyma through BBB, we labeled nanoparticles with Dil and injected to mice intravenously. Brains were collected and sliced. As shown in Fig. 6A, red indicatesd the fluorescently labeled LNP and green indicated blood vessels. The nanoparticles crossed the blood vessels and entered the brain parenchyma. The amount of Lpc-BoSA/CSO entering the brain parenchyma was 4.21 times that of Lec-SA (Fig. 6B, $P < 0.001$).

3.7. *Multi-functionalized nanoparticles improved motor symptoms of PD mice*

PD is an age-related neurodegenerative disease. The degeneration degree of substantia nigra dopaminergic neurons and the microenvironment around the lesion in mice of different ages may vary greatly during MPTP induction. In our study, 15-month-old aged mice were used to induce PD model with MPTP. Lpc-BoSA/CSO-Exe, Lpc-BoSA/Exe, Lpc-SA/Exe, Lec-BoSA/Exe and Lec-SA/Exe, with Exe dose of 0.3 mg/kg, were injected intravenously. Exe was injected subcutaneously. The experimental plan is shown in Fig. 7A.

Three weeks after dosing, mice were subjected to behavioral evaluation. In the open field test (OFT), PD mice were afraid of the new open environment and mainly moved in the peripheral area, so they tended to have shorter distances, longer stationary time and rarely moved in the center zone. As seen in Fig. 7B and 7C, mice in Lpc-BoSA/CSO-Exe group had the longest travel distance ($P < 0.0001$), shortest

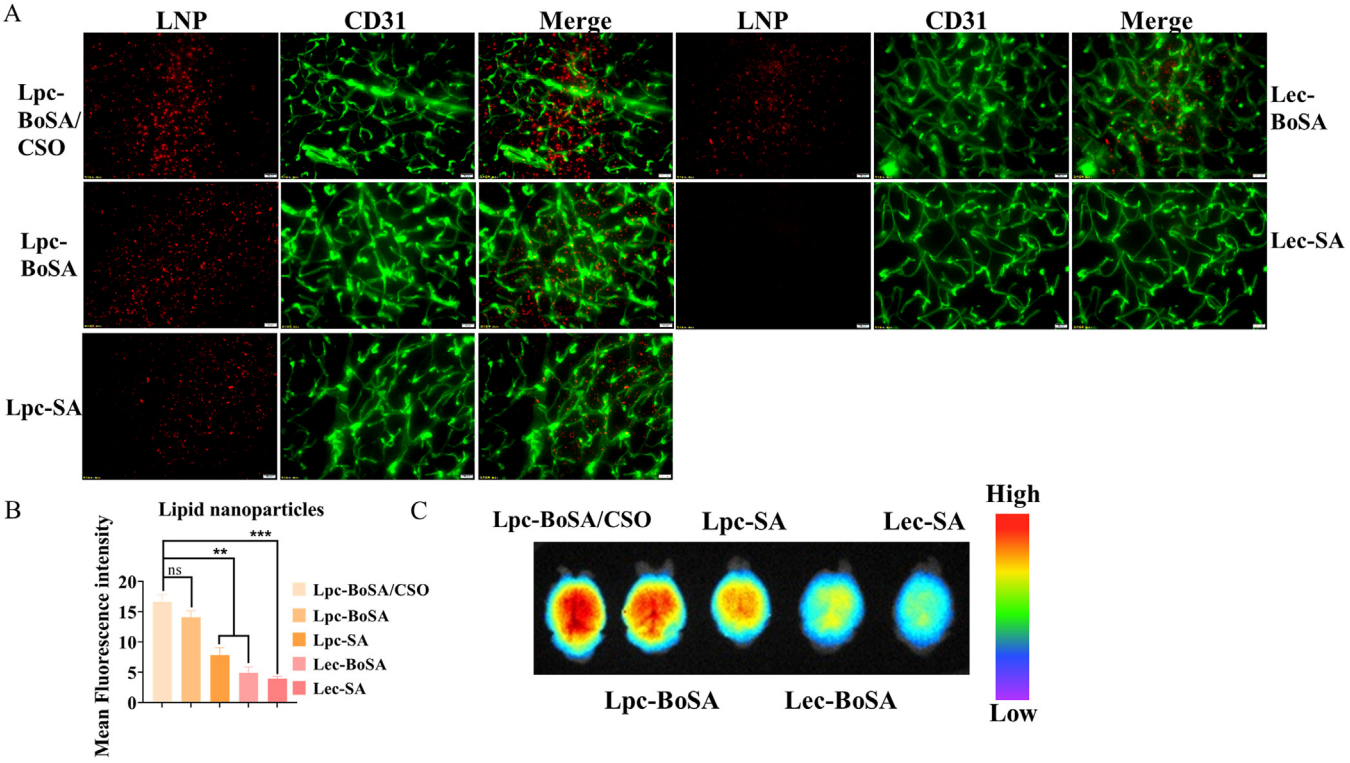

Fig. 6 – LNP entering the brain parenchyma. (A) Substantia nigra pars compacta tissue sections of mice in different groups. CD31-labeled blood vessels are shown in green, and Dil-labeled LNP in red; (B) Semi-quantification of fluorescence signal in Fig. A ($n = 3$, $^{**}P < 0.01$, $^{***}P < 0.001$); (C) *In vivo* images of LNP distribution in the brain (upper image). *In vivo* distribution of Lpc-BoSA/CSO in heart, liver, spleen, lung and kidneys.

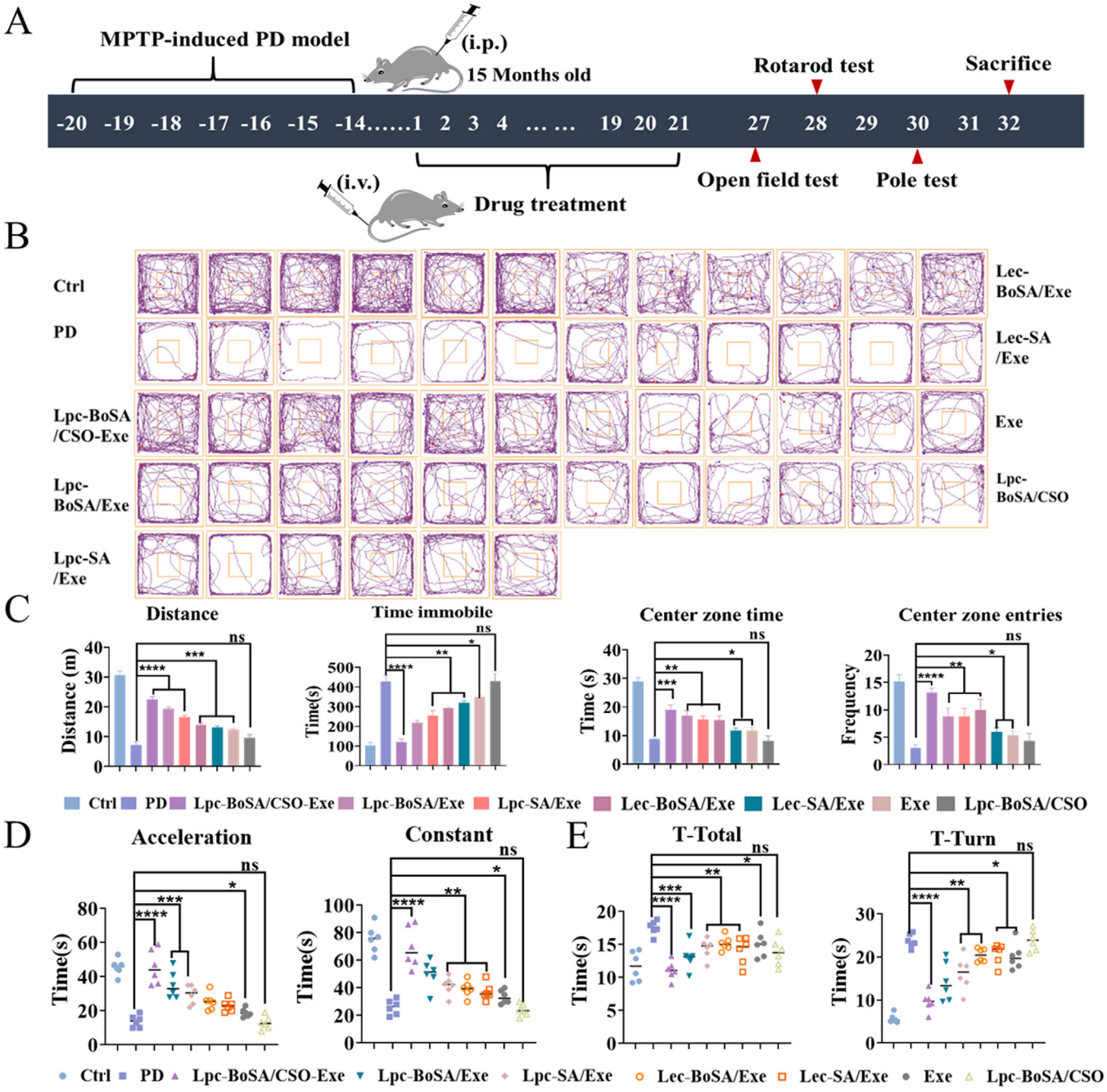

Fig. 7 – Multi-functionalized Exe LNP improved motor symptoms of PD mice. (A) Experimental arrangement of the dosing design; (B) Movement trajectories of mice in OFT; (C) Statistical plot of movement distance, stationary time, central zone time and central zone entries of mice in OFT; (D) Statistical plots of time on the rod in accelerated mode (left) and constant mode (right) in the rotarod test; (E) Statistical plots of time mice took from the top to the bottom (left) and time mice took to complete the turn (right) in the pole test. ($n = 6$, *$P < 0.05$, **$P < 0.01$, ***$P < 0.001$ and ****$P < 0.0001$).

immobile time ($P < 0.0001$), and tended to stay in the center of the field ($P < 0.0001$) compared to PD mice. In rotarod test, marked motor deficits were seen in PD mice with a significant drop in the time they remained on the rod compared to the control. While there was a remarkable drop in the number of falls for mice in Lpc-BoSA/CSO-Exe group at both constant and acceleration speed mode ($P < 0.0001$), which suggested an improved motor coordination (Fig. 7D). In pole test, PD mice tended to have longer T-Total and T-Turn. However, there was a significant reduction in the time of mice in Lpc-BoSA/CSO-Exe group ($P < 0.0001$), which indicated a meliorative motor coordination (Fig. 7E). Improvement in motor symptoms suggested that functionalized nanoparticles entered the brain parenchyma through transcytosis and paracellular

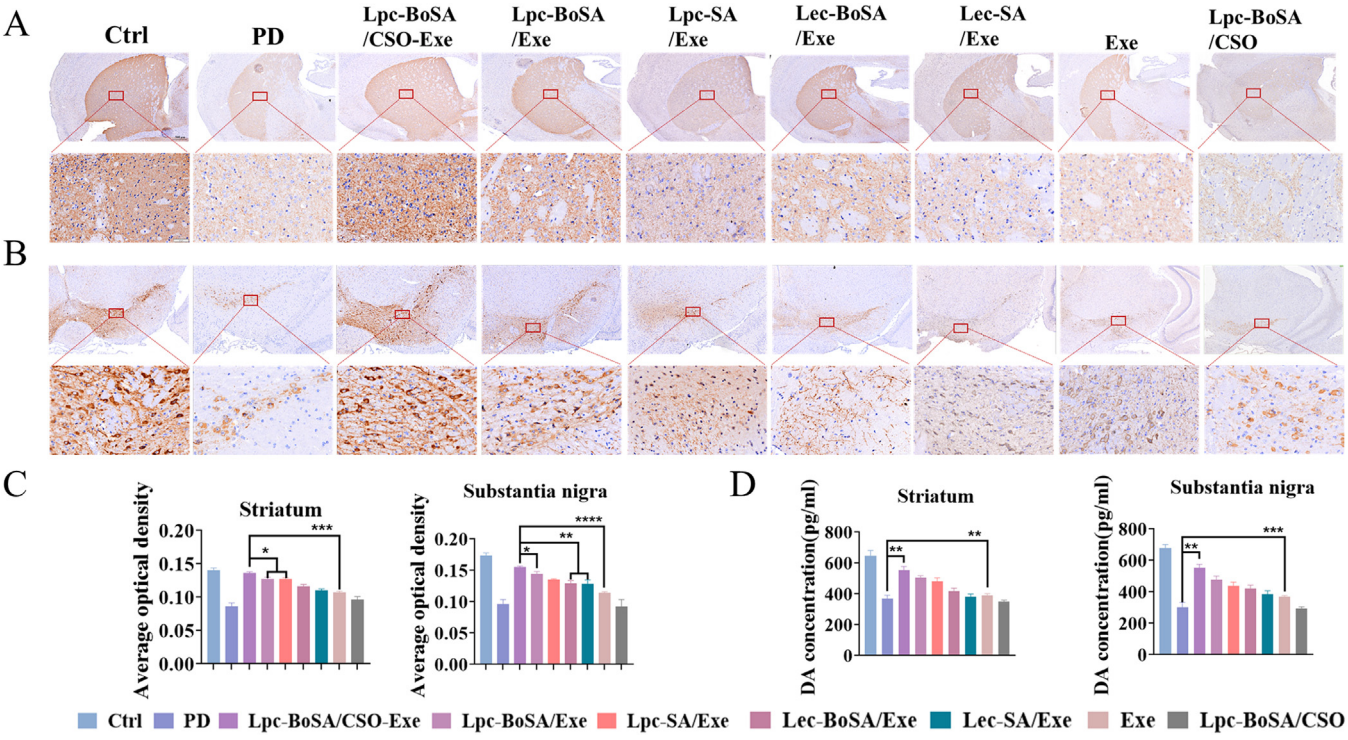

Fig. 8 – Multi-functionalized Exe LNP rescued TH-positive neurons of PD mice. (A) Expression of TH in striatum of mice (upper graph scale bar: 500 μm, lower graph scale bar: 50 μm); (B) Expression of TH in SNpc; (C) Quantification of TH in striatum (left) and SNpc (right) of mice; (D) Quantification of dopamine content in striatum (left) and SNpc (right) of mice. (n = 6, *P < 0.05, **P < 0.01, ***P < 0.001 and ****P < 0.0001).

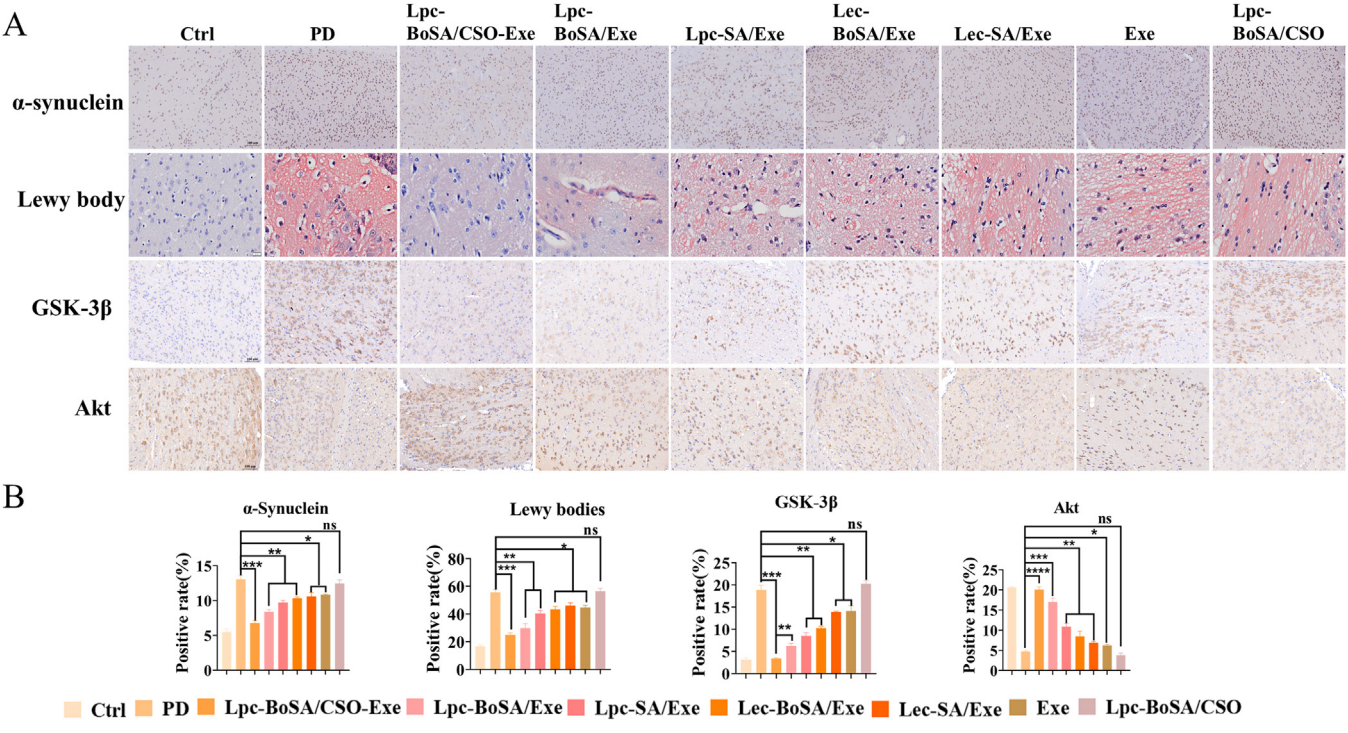

Fig. 9 – Exe LNP reduced α-synuclein formation through AKT/GSK-3β pathway. (A) α-synuclein, Lewy body, GSK-3β and AKT expression of mice in each treatment group; (B) Statistical plots of α-synuclein, Lewy body, GSK-3β and AKT expression. (n = 6, *P < 0.05, **P < 0.01, ***P < 0.001 and ****P < 0.0001).

pathways via increased BBB permeability by borneol, released Exe responsively in the PD foci microenvironment.

3.8. *Multi-functionalized LNP restored dopaminergic neurons and reduced amyloid protein production of PD mice*

The dominant pathological feature of PD is the degeneration and death of TH-positive neurons in the SNpc of the midbrain, which causes a significant decrease in dopamine (DA) content in the Cpu. Mice were anesthetized and brains were excised for measurement of TH and DA. Representative TH staining is shown in Fig. 8A and 8B. TH expression in striatum ($P < 0.001$) and SNpc ($P < 0.0001$) in Lpc-BoSA/CSO-Exe group were significantly higher than that of Exe group, which suggested under the dual effect of BBB targeting and permeability increasing, Exe efficiently entered the brain parenchyma and was released responsively to restore dopamine neurons (Fig. 8C). Furthermore, DA content of mice in Lpc-BoSA/CSO-Exe group was the highest (Fig. 8D). The above results confirmed Exe could rescue dopamine neurons and Lpc-BoSA/CSO-Exe enhanced the therapeutic effect of Exe.

In our study, we used 15-month-old male C57BL/6 and detected accumulated α-synuclein as well as Lewy bodies. As seen in Fig. 9A, mice in PD group had obvious staining of α-synuclein and Lewy body. α-synuclein in Lpc-BoSA/CSO-Exe group was decreased to 51.85% of that in PD group (Fig. 9B, $P < 0.001$).

In addition, we performed Congo red staining on mouse brain tissue sections to further detect the content of Lewy bodies. Lewy bodies are partially hollow radial amyloid fibrils that combine with Congo red to form red complexes. As shown in Fig. 9A, PD mice had densities of amyloid fibril deposition in the brain. The reduction of amyloid fibrils in group Lpc-BoSA/CSO-Exe was the most prominent, down to 44.72% of that in PD group (Fig. 9B, $P < 0.001$).

3.9. *Exe LNP reduced α-synuclein accumulation through the AKT /GSK-3β pathway*

The pathological hallmark of PD is intraneuronal Lewy Body composed predominantly of aggregated α-synuclein, which is elevated in post-mortem PD brains. Preventing the formation or promoting the clearance of intracellular α-synuclein denotes promising disease-modifying strategies for PD therapy. Hence, we detected the expression of AKT and GSK-3β in brain tissue of mice. As expected, AKT

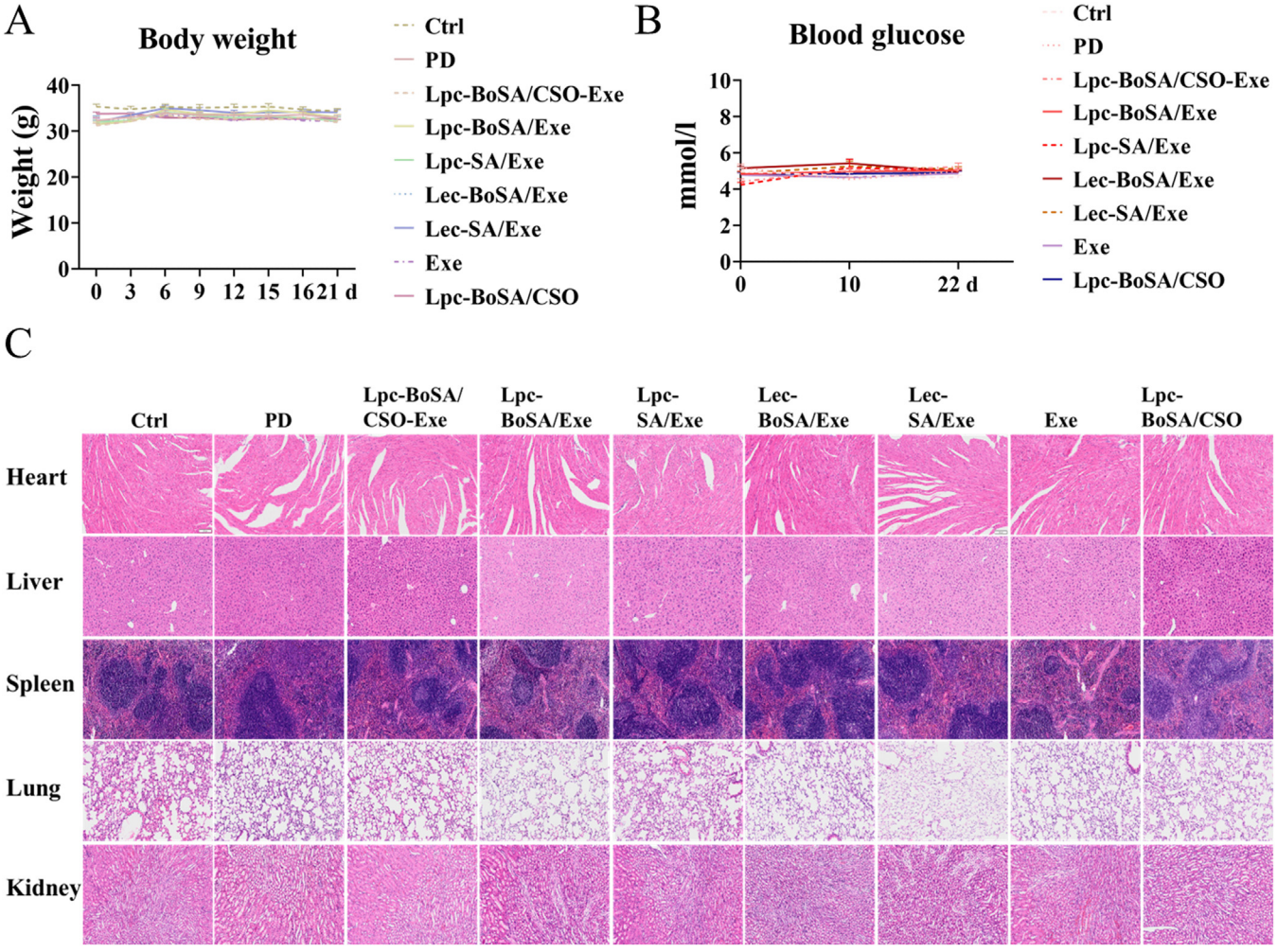

Fig. 10 – *In vivo* safety assessment of LNP. (A) Body weight of mice in each treatment group; (B) Blood glucose levels of mice; (C) H&E staining results of mouse heart, liver, spleen, lung, and kidney (scale bar: 100 μm, $n = 6$).

expression was significantly reduced in PD mice, leading to upregulation of downstream GSK-3β expression and ultimately promoting accumulation of α-synuclein (Fig. 9A). The expression of AKT in Lpc-BoSA/CSO-Exe group was significantly up-regulated and was 4.23 times that of PD group (Fig. 9B, $P < 0.0001$). Accordingly, GSK-3β expression remarkably decreased, down to 18.41% that of PD group (Fig. 9B, $P < 0.001$). These experiments suggested that Exe reduced α-synuclein formation through the AKT/GSK-3β pathway to exert disease-modifying efficacy, thus preventing or slowing down progressive neurodegeneration in PD. Exe encapsulated in Lpc-BoSA/CSO could enter the brain parenchyma more efficiently and achieve greater efficacy.

During the drug administration, we continuously monitored the mice's body weight and blood glucose. The results showed no significant abnormalities (Fig. 10A and 10B). H&E staining of heart, liver, spleen, lung and kidney of mice in each group was normal (Fig. 10C), indicating that multi-functionalized LNP had good safety *in vivo*.

4. Conclusion

We fabricated multi-functionalized LNP with BBB targeting, permeability-increasing, as well as responsive drug release functions. Lpc-BoSA/CSO-Exe effectively promoted the efficient entry of Exe into the brain parenchyma, repaired dopaminergic neurons, reduced α-synuclein production, and prevented or alleviated the progressive degeneration of PD, which effectively solved the difficulty of PD clinical treatment being unable to alleviate the progressive degeneration and the intractable problem for drugs to cross the BBB. As a promising disease-modifying therapy, Lpc-BoSA/CSO-Exe brings benefits to Parkinson's patients.

Conflicts of interest

The authors declare no competing interest.

Acknowledgments

We thank the National Natural Science Foundation of China (grant nos. 81973267) and Natural Science Foundation of Zhejiang Province (grant nos. LD19H300001).

REFERENCES

[1] Poewe W, Seppi K, Tanner CM, Halliday GM, Brundin P, Volkmann J, et al. Parkinson disease. Nat Rev Dis Primers 2017;3:17013.
[2] Bloem BR, Okun MS, Klein C. Parkinson's disease. The Lancet 2021;397(10291):2284–303.
[3] Erbil D, Eren CY, Demirel C, Küçüker MU, Solaroğlu I, Eser HY. GLP-1's role in neuroprotection: a systematic review. Brain Inj 2019;33(6):734–819.
[4] Athauda D, Foltynie T. The glucagon-like peptide 1 (GLP) receptor as a therapeutic target in Parkinson's disease: mechanisms of action. Drug Discov Today 2016;21(15):802–18.
[5] Jankovic J. Exenatide–a drug for diabetes and Parkinson disease? Nat Rev Neurol 2017;13(11):643–4.
[6] Vijiaratnam N, Girges C, Auld G, Chau M, Maclagan K, King A, et al. Exenatide once weekly over 2 years as a potential disease-modifying treatment for Parkinson's disease: protocol for a multicentre, randomised, double blind, parallel group, placebo controlled, phase 3 trial: the 'Exenatide-PD3'study. BMJ Open 2021;11(5):e047993.
[7] Segarra M, Aburto MR, Acker-Palmer A. Blood–brain barrier dynamics to maintain brain homeostasis. Trends Neurosci 2021;44(5):393–405.
[8] Langen UH, Ayloo S, Gu C. Development and cell biology of the blood-brain barrier. Annu Rev Cell Dev Biol 2019;35:591–613.
[9] Greene C, Hanley N, Campbell M. Claudin-5: gatekeeper of neurological function. Fluids Barriers CNS 2019;16(1):1–15.
[10] Tan L, Wang Y, Jiang Y, Wang R, Zu J, Tan R. Hydroxysafflor yellow A together with blood–brain barrier regulator lexiscan for cerebral ischemia reperfusion injury treatment. ACS Omega 2020;5(1):19151–64.
[11] Wu Y, Wang S, Shang L, Zhang H, Qin J, Ren Y, et al. Effect of borneol as a penetration enhancer on brain targeting of nanoliposomes: facilitate direct delivery to neurons. Nanomedicine 2018;13(21):2709–27.
[12] Barton SM, Janve VA, McClure R, Anderson A, Matsubara JA, Gore JC, et al. Lipopolysaccharide induced opening of the blood brain barrier on aging 5XFAD mouse model. J Alzheimer's Dis 2019;67(21):503–13.
[13] Han L. Modulation of the blood–brain barrier for drug delivery to brain. Pharmaceutics 2021;13(12):2024.
[14] Terstappen GC, Meyer AH, Bell RD, Zhang W. Strategies for delivering therapeutics across the blood–brain barrier. Nat Rev Drug Discov 2021;20(5):362–83.
[15] Bubb KJ, Aubdool AA, Moyes AJ, Lewis S, Drayton JP, Tang O, et al. Endothelial C-type natriuretic peptide is a critical regulator of angiogenesis and vascular remodeling. Circulation 2019;139(13):1612–28.
[16] Chu C, Jablonska A, Lesniak WG, Thomas AM, Lan X, Linville RM, et al. Optimization of osmotic blood-brain barrier opening to enable intravital microscopy studies on drug delivery in mouse cortex. J Control Release 2020;317:312–21.
[17] Mugisho OO, Robilliard LD, Nicholson LF, Graham ES, O'Carroll SJ. Bradykinin receptor-1 activation induces inflammation and increases the permeability of human brain microvascular endothelial cells. Cell Biol Int 2020;44(1):343–51.
[18] Peng X, Luo Z, He S, Zhang L, Li Y. Blood-brain barrier disruption by lipopolysaccharide and sepsis-associated encephalopathy. Front Cell Infect Microbiol 2021;11:1083.
[19] Burks SR, Kersch CN, Witko JA, Pagel MA, Sundby M, Muldoon LL, et al. Blood–brain barrier opening by intracarotid artery hyperosmolar mannitol induces sterile inflammatory and innate immune responses. PNAS 2021;118(18):e2021915118.
[20] Zhang J, Liu SL, Wang H, Shi LY, Li JP, Jia LJ, et al. The effects of borneol on the pharmacokinetics and brain distribution of tanshinone IIA, salvianolic acid B and ginsenoside Rg1 in Fufang Danshen preparation in rats. Chin J Nat Med 2021;19(2):153–60.
[21] Kim S, Kim JH, Seok SH, Park ES. Enhanced permeability and oral absorption of Panax notoginseng saponins by borneol. J Drug Deliv Sci Technol 2021;66:102819.
[22] Lv L, Li X, Qian W, Li S, Jiang Y, Xiong Y, et al. Enhanced anti-glioma efficacy by borneol combined with CGKRK-modified paclitaxel self-assembled redox-sensitive nanoparticles. Front Pharmacol 2020;11:558.

[23] Li JY, Wang JX, Li QH, Li XF, Xiao JP, Li SS, et al. Natural borneol enhances the anti-cerebral ischaemia efficacy of formononetin in MCAO/R rats by promoting its delivery in the brain. J Pharm Pharmacol 2022;74(11):1598–608.
[24] Lin JF, Liu YS, Huang YC, Chi CW, Tsai CC, Tsai TH, et al. Borneol and tetrandrine modulate the blood–brain barrier and blood–tumor barrier to improve the therapeutic efficacy of 5-fluorouracil in brain metastasis. Integr Cancer Ther 2022;21:15347354221077682.
[25] Kulkarni M, Sawant N, Kolapkar A, Huprikar A, Desai N. Borneol: a promising monoterpenoid in enhancing drug delivery across various physiological barriers. AAPS PharmSciTech 2021;22(4):145.
[26] Yin Y, Cao L, Ge H, Duanmu W, Tan L, Yuan J, et al. L-Borneol induces transient opening of the blood–brain barrier and enhances the therapeutic effect of cisplatin. Neuroreport 2017;28(9):506–13.
[27] Jan A, Gonçalves NP, Vaegter CB, Jensen PH, Ferreira N. The prion-like spreading of alpha-synuclein in Parkinson's disease: update on models and hypotheses. Int J Mol Sci 2021;22(15):8338.
[28] Du XY, Xie XX, Liu RT. The role of α-synuclein oligomers in Parkinson's disease. Int J Mol Sci 2020;21(22):8645.
[29] Ferman TJ, Aoki N, Boeve BF, Aakre JA, Kantarci K, Graff-Radford J, et al. Subtypes of dementia with Lewy bodies are associated with α-synuclein and tau distribution. Neurology 2020;95(2):e155–65.
[30] Kofoed RH, Betzer C, Ferreira N, Jensen PH. Glycogen synthase kinase 3 β activity is essential for Polo-like kinase 2-and Leucine-rich repeat kinase 2-mediated regulation of α-synuclein. Neurobiol Dis 2020;136:104720.
[31] Glotfelty EJ, Olson L, Karlsson TE, Li Y, Greig NH. Glucagon-like peptide-1 (GLP-1)-based receptor agonists as a treatment for Parkinson's disease. Expert Opin Investig Drugs 2020;29(6):595–602.
[32] Manning BD, Toker A. AKT/PKB signaling: navigating the network. Cell 2017;169(3):381–405.
[33] Guttuso T Jr, Andrzejewski KL, Lichter DG, Andersen JK. Targeting kinases in Parkinson's disease: a mechanism shared by LRRK2, neurotrophins, exenatide, urate, nilotinib and lithium. J Neurol Sci 2019;402:121–30.
[34] Yang JL, Lin YT, Chen WY, Yang YR, Sun SF, Chen SD. The neurotrophic function of glucagon-like peptide-1 promotes human neuroblastoma differentiation via the PI3K-AKT axis. Biology (Basel) 2020;9(3):348.
[35] Xiong RR, Ling GX, Zhang YQ, Guan JB, Zhang P. Nucleic acid delivery by ionizable nanocarriers for brain disease treatment. Brain-X 2023;1(1):e7.
[36] Zhang YQ, Guo RR, Chen YH, Li TC, Du WZ, Xiang RW, et al. Ionizable drug delivery systems for efficient and selective gene therapy. Mil Med Res 2023;10(1):9.
[37] Ju X, Miao T, Chen H, Ni J, Han L. Overcoming Mfsd2a-Mediated Low transcytosis to boost nanoparticle delivery to brain for chemotherapy of brain metastases. Adv Healthc Mater 2021;10(9):2001997.
[38] Wang JZ, Xiao N, Zhang YZ, Zhao CX, Guo XH, Lu LM. Mfsd2a-based pharmacological strategies for drug delivery across the blood–brain barrier. Pharmacol Res 2016;104:124–31.
[39] Nguyen LN, Ma D, Shui G, Wong P, Cazenave-Gassiot A, Zhang X, et al. Mfsd2a is a transporter for the essential omega-3 fatty acid docosahexaenoic acid. Nature 2014;509(7501):503–6.
[40] Richard I, Thibault M, De Crescenzo G, Buschmann MD, Lavertu M. Ionization behavior of chitosan and chitosan–DNA polyplexes indicate that chitosan has a similar capability to induce a proton-sponge effect as PEI. Biomacromolecules 2013;14(6):1732–40.
[41] Lavanya K, Chandran VS, Balagangadharan K, Selvamurugan N. Temperature-and pH-responsive chitosan-based injectable hydrogels for bone tissue engineering. Mater Sci Eng 2020;111:110862.
[42] Cooley M, Sarode A, Hoore M, Fedosov DA, Mitragotri S, Gupta AS. Influence of particle size and shape on their margination and wall-adhesion: implications in drug delivery vehicle design across nano-to-micro scale. Nanoscale 2018;10(32):15350–64.
[43] . The pharmacopoeia of People's Republic of China, 1. Beijing: China Medical Science Press; 2020. p. 201. (Borneol).
[44] Trist BG, Hare DJ, Double KL. Oxidative stress in the aging substantia Nigra and the etiology of Parkinson's disease. Aging Cell 2019;18(6):e13031.
[45] Li H, Xin C, Zhang G, Han X, Qin W, Zhang CW, et al. A mitochondria-targeted two-photon fluorogenic probe for the dual-imaging of viscosity and H_2O_2 levels in Parkinson's disease models. J Mater Chem B 2019;7(27):4243–51.